

# Correlated electron tunneling through two separate quantum dot systems with strong capacitive interdot coupling

A. Hübel<sup>1</sup>, K. Held<sup>1,2</sup>, J. Weis<sup>1</sup>, and K. v. Klitzing<sup>1</sup>

<sup>1</sup> *Max-Planck-Institut für Festkörperforschung, Heisenbergstr. 1, D-70569 Stuttgart, Germany and*

<sup>2</sup> *Institute for Solid State Physics, Vienna University of Technology, 1040 Vienna, Austria*

(Dated: July 21, 2021)

A system consisting of two independently contacted quantum dots with strong electrostatic interaction shows interdot Coulomb blockade when the dots are weakly tunnel coupled to their leads. It is studied experimentally how the blockade can be overcome by correlated tunneling when tunnel coupling to the leads increases. The experimental results are compared with numerical renormalization group calculations using predefined (measured) parameters. Our results indicate Kondo correlations due to the electrostatic interaction in this double quantum dot system.

PACS numbers: 73.63.Kv, 72.15.Qm, 71.45.-d

Electrical transport through a quantum dot at low temperature is dominated by the electron-electron interaction, leading to Coulomb blockade and single-electron charging effects [1]. The spin as an internal degree of freedom causes under certain circumstances a Kondo correlated state to form between the quantum dot and its source and drain leads, overcoming the Coulomb blockade with decreasing temperature [2]. The Anderson impurity model not only provides a simplified, yet appropriate description for this particular effect but, at the same time, it is the basic model for a quantum dot system, i.e., a single localized orbital tunnel coupled to leads [3]. Two independently contacted quantum dots with purely capacitive interaction can be labeled by a pseudo-spin index and can therefore be described as another realization of the Anderson impurity model [4]. Theory predicts that correlations should lift the Coulomb blockade where an electrostatic degeneracy exists between states with  $(N_1, N_2)$  and  $(N_1 \pm 1, N_2 \mp 1)$  electrons on the two dots. Experimentally one would observe the Kondo correlations under such degeneracy conditions upon enhancing the tunnel couplings of the dots to the leads or lowering the temperature. When the spin is included, Kondo physics with SU(4) symmetry can be present [5]. Experimental results on cylindrical quantum dots [6] and carbon nanotubes [7] have been interpreted in terms of an SU(4) spin-orbital Kondo effect. However the tunneling paths via the two orbitals were not separately accessible to experiment, and therefore assumptions about them had to be made. In contrast, the setup of separate quantum dot systems with interdot capacitive coupling allows one to study the (pseudo)spin-polarized currents and therefore the Kondo correlations in a controlled way, provided the conductances through the two quantum dots can be monitored independently and for different parameter combinations. Several experiments have examined the behavior of such samples at weak tunnel couplings, where single-electron tunneling is an appropriate description [8], showing the expected honeycomb-like charge stability diagram with less pronounced capacitive interdot coupling. Two

vertically stacked quantum dot systems show strong interdot capacitive coupling, and indications of Kondo correlations have been observed, however the structure lacks full control over the tunnel couplings [9].

In this letter we use a double quantum dot system in lateral arrangement with strong capacitive interdot interaction and fully tunable tunnel couplings [10]. The regions where transport is dominated by interdot correlations are well-resolved, and we study experimentally the transition from weak to strong tunnel coupling. The conductances and the parameters of both quantum dots are measured independently, so we can directly compare with numerical renormalization group (NRG) calculations identifying Kondo-like correlations.

A scanning electron microscope (SEM) image of our sample is shown in the inset of Fig. 1. Its design concept and its fabrication have been described elsewhere in more detail [10]. We use a GaAs/Al<sub>0.33</sub>Ga<sub>0.67</sub>As heterostructure with a two-dimensional electron system, located at the heterojunction 50 nm below the surface (electron density:  $3.2 \times 10^{11} \text{ cm}^{-2}$ , mobility:  $3.0 \times 10^5 \text{ cm}^2 \text{ V}^{-1} \text{ s}^{-1}$  at 4.2 K). First, we define a floating metallic top gate by electron beam lithography. In the second step, 50 nm deep trenches are etched around this top gate in a SiCl<sub>4</sub> plasma. The depletion regions around these trenches define the two quantum dots. We label them ‘u’ and ‘d’, for ‘up’ and ‘down’ in Fig. 1. Each quantum dot has its own source and drain leads, so we can independently measure their differential conductances  $dI_D^{(u)}/dV_{DS}^{(u)}$  and  $dI_D^{(d)}/dV_{DS}^{(d)}$  [16]. Furthermore, each of the four tunnel barriers is tunable by one of the adjacent gates 1 to 4. It was tested experimentally that the bridge between the two quantum dots carrying the top gate is entirely depleted, so no current can flow between the dots and the coupling is purely capacitive. The top gate is needed to reach a large interdot capacitance leading to a large ratio between the interdot Coulomb energy  $U$  and the intradot charging energies  $E_{Cu}$  and  $E_{Cd}$  [17].

At our base temperature of 25 mK, the conductances at small source-drain voltages show a honeycomb-like struc-

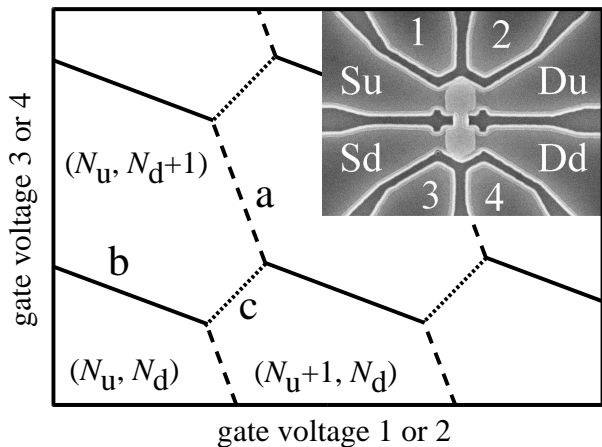


FIG. 1: Scheme of charge stability in a double quantum dot system as a function of two gate voltages, reflecting the characteristic honeycomb-like structure. At weak tunnel couplings, single-electron transport is possible through one of the dots on hexagon edges of type *a* and *b*, respectively. Correlations between the quantum dots can lead to transport on type *c* edges for enhanced tunnel couplings. Inset: SEM image with labeled electrodes and floating top gate in the center.

ture as a function of two gate voltages [10], as expected from a simple electrostatic model [11]. Fig. 1 gives the basic definitions to be used for its description. Each possible combination  $(N_u, N_d)$  of occupation numbers is stable inside a hexagonal area in the parameter space spanned by the two gate voltages. At tunnel couplings  $\Gamma_u$  and  $\Gamma_d$  much smaller than the thermal energy  $k_B T$ , only single-electron tunneling is possible, and only on those hexagon edges where exactly one quantum dot changes its occupation number (edges of type *a* and *b*). In contrast, no conductance is found on type *c* edges where both occupation numbers must change simultaneously. There, the interdot Coulomb blockade prevents single-electron tunneling. Near the common pinch-off point of all four tunnel barriers, we find  $U \approx 0.26$  meV, and  $U/E_{Cu} \approx U/E_{Cd} \approx 1/3$ . These values decrease as one opens the tunnel barriers because of increasing dot-lead capacitances [12].

As a measure of the tunnel couplings, we take the full widths at half maximum of the Coulomb peaks on the type *a* and type *b* edges. In order to convert these values (measured in units of a gate voltage) into energies, we determine the capacitive lever arm between the gate voltage and the quantum dot's addition energy by finite source-drain voltage measurements as described in [12]. The sharp conductance peaks of the weakly tunnel coupled quantum dots are used in order to precisely evaluate the energy scale, which is then transferred to the strongly coupled system. In the experiment, the tunnel couplings are usually large compared to  $k_B T$  at the base temperature of 25 mK, which means that temperature broadening effects are negligible; for type *a* or type *b* edges the conductance peaks show a lineshape which is approxi-

mately Lorentzian in most cases. The interesting regions we will focus on in the rest of this letter are obviously the edges of type *c*. Here, we cannot start from the simple single-electron tunneling picture because of the interdot Coulomb blockade.

Fig. 2(a) shows a region with small tunnel couplings in more detail. Finite conductances can be seen only on the type *a* and type *b* edges, so single-electron tunneling provides a qualitatively sufficient explanation. Fig. 2(b) shows a situation in which one of the dots is much more strongly tunnel coupled to its leads, while the other one remains weakly coupled. A sharp conductance peak is observed for the weakly coupled dot that follows a continuous curve, so the interdot Coulomb blockade is lifted. The peak amplitude is smallest at the turning point of the position curve, and the lineshape of the conductance peaks was checked to be Lorentzian for all line cuts along the  $V_1$  direction (horizontal). Far from the turning point, the curve becomes straight as a function of the gate voltages, and we can then take the position of the conductance peak maximum as a definition of the type *a* honeycomb edges. A different behavior is observed for the strongly coupled dot: The conductance plot appears to be divided into two half planes. On each side, the conductance peaks are simply described by a Lorentzian whose center defines the type *b* honeycomb edge. A narrow, step-like transition occurs in between. It is located at the same position where we observe the conductance peak in the weakly coupled dot.

For the following discussion, we describe the two dots with an Anderson impurity model which has a single, spin-degenerate quantum level in each dot:

$$\begin{aligned} \hat{H} = & \sum_{i \in \{u, d\}} (\varepsilon_i \cdot \hat{n}_i + E_{Ci} \cdot \hat{n}_{i\uparrow} \hat{n}_{i\downarrow}) + U \cdot \hat{n}_u \hat{n}_d \\ & + \sum_{Ri, k, \sigma} \varepsilon_k \cdot \hat{c}_{Ri, k, \sigma}^\dagger \hat{c}_{Ri, k, \sigma} \\ & + \sum_{Ri, k, \sigma} \left( t_{Ri} \cdot \hat{a}_{i, \sigma}^\dagger \hat{c}_{Ri, k, \sigma} + \text{h.c.} \right). \end{aligned} \quad (1)$$

Here,  $\hat{a}_{i, \sigma}^\dagger$  ( $\hat{a}_{i, \sigma}$ ) create (annihilate) an electron with spin  $\sigma \in \{\downarrow, \uparrow\}$  in dot  $i \in \{u, d\}$ ;  $\hat{n}_{i, \sigma} = \hat{a}_{i, \sigma}^\dagger \hat{a}_{i, \sigma}$  and  $\hat{n}_i = \hat{n}_{i, \uparrow} + \hat{n}_{i, \downarrow}$ , are the corresponding number operators;  $\varepsilon_u$  and  $\varepsilon_d$  denote the addition energies of the dots relatively to the source Fermi level, which shift linearly with applied gate voltages;  $\hat{c}_{Ri, k, \sigma}^\dagger$  is the creation operator for an electron in lead  $R \in \{S, D\}$  of system  $i \in \{u, d\}$  with wavenumber  $k$ , spin  $\sigma$  and energy  $\varepsilon_k$ . Finally,  $t_{Ri}$  denotes the corresponding spin-independent tunnel matrix element, which translates into a tunnel rate  $\Gamma_i = 2\pi\rho \cdot (t_{Si}^2 + t_{Di}^2)$  where  $\rho$  is the density of states in the leads.

To get a simple physical picture, we neglect, in a first approximation, charge fluctuations in the (much) more weakly coupled dot, setting  $\Gamma_u = 0$ . Since no spin-Kondo

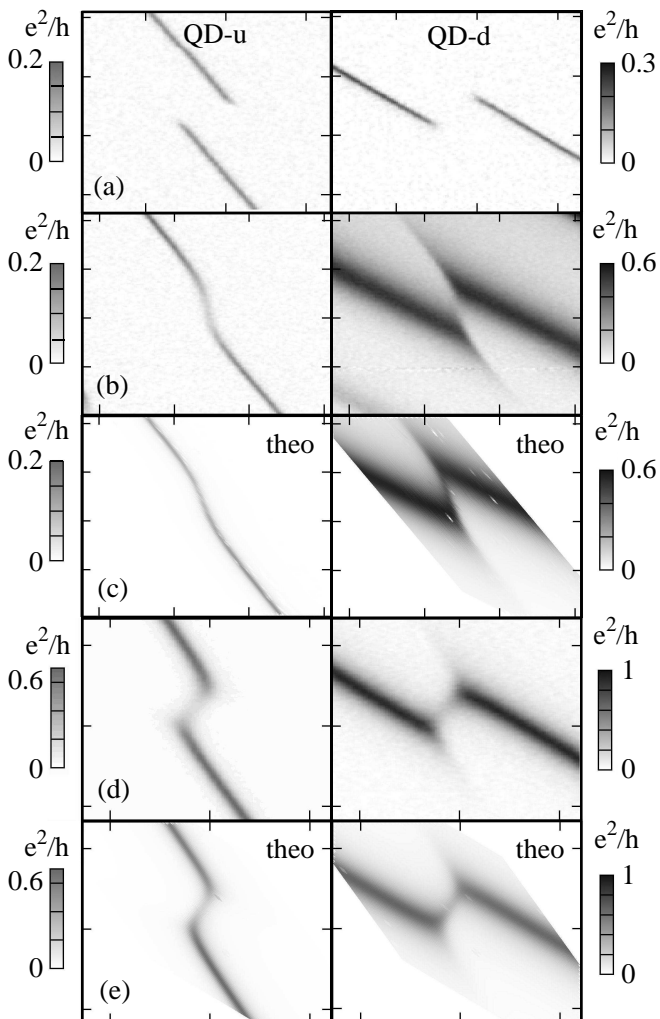


FIG. 2: The conductances of quantum dots ‘u’ (left) and ‘d’ (right) in greyscale at 25 mK around three type *c* lines for different tunnel couplings. Horizontal axes:  $V_{1,2}$ ; vertical axes:  $V_{3,4}$  in steps of 2 mV. (a),(b),(d) are measured, (c),(e) are calculated by using parameters extracted from (b),(d), respectively.  $\Gamma_u = \Gamma_d = 25 \mu\text{eV}$  and  $U = 260 \mu\text{eV}$  in (a);  $\Gamma_u = 25 \mu\text{eV}$ ,  $\Gamma_d = 110 \mu\text{eV}$ , and  $U = 140 \mu\text{eV}$  in (b);  $\Gamma_u = 32 \mu\text{eV}$ ,  $\Gamma_d = 59 \mu\text{eV}$ , and  $U = 163 \mu\text{eV}$  in (d).

effect was observed in the adjacent Coulomb blockade valleys, and the intradot charging energies are the largest parameters in the system ( $E_{Cu} \approx E_{Cd} \approx 0.6 \text{ meV}$  in Fig. 2(b,d) and 3(b,c) obtained from measurements of the Coulomb blockade diamonds), we further neglect double occupation of the individual dots and drop the  $E_{Ci}$  terms and the spin indices in Eq. (1). The description of the double-dot ground state then reduces to a resonant tunneling Hamiltonian for the strongly coupled quantum dot, predicting a Lorentzian spectral density of width  $\Gamma_d$  on this dot [13]. However, the resonant state now has two possible addition energies,  $\varepsilon_d$  and  $\varepsilon_d + U$ , depending on the (fixed) occupation number  $N_u \in \{0, 1\}$  of the weakly tunnel coupled dot. Like in the electrostatic model [11],

we assume that the system takes the state of minimal electrostatic energy  $E$ , which is given by the expectation value of  $\varepsilon_u \cdot \hat{n}_u + \varepsilon_d \cdot \hat{n}_d + U \cdot \hat{n}_u \hat{n}_d$ :

$$E(N_u) = \varepsilon_u \cdot N_u + \left( \varepsilon_d + U \cdot N_u \right) \times \left[ \frac{1}{2} - \frac{1}{\pi} \cdot \arctan \frac{\varepsilon_d + U \cdot N_u}{\Gamma_d/2} \right]. \quad (2)$$

Conductance through the weakly coupled dot is now possible for  $E(N_u = 1) = E(0)$ , even if charge fluctuations ( $\Gamma_u$ ) are very small. This yields a relation between  $\varepsilon_d$  and  $\varepsilon_u$ , which we express after substituting  $\varepsilon_i$  by  $\varepsilon'_i - U/2$  as

$$\varepsilon'_u = \left( \varepsilon'_d + U/2 \right) \cdot \frac{1}{\pi} \arctan \frac{\varepsilon'_d + U/2}{\Gamma_d/2} - \left( \varepsilon'_d - U/2 \right) \cdot \frac{1}{\pi} \arctan \frac{\varepsilon'_d - U/2}{\Gamma_d/2}. \quad (3)$$

Note the point symmetry around  $\varepsilon'_d = \varepsilon'_u = 0$ . Only the ratios  $\varepsilon'_i/U$  and  $\Gamma_d/U$  enter, which can be measured to within a few per cent. The two quantities  $\varepsilon'_i/U$  are linear functions of the gate voltages entirely determined by capacitance ratios, i.e. the slopes of the honeycomb edges. By evaluating Fig. 2(b), we get the transformation relation

$$\begin{pmatrix} V_1 - V_1^{(0)} \\ V_3 - V_3^{(0)} \end{pmatrix} / \text{mV} = \begin{pmatrix} -1.62(0) & 1.74(3) \\ 1.26(0) & -3.19(8) \end{pmatrix} \begin{pmatrix} \varepsilon'_u/U \\ \varepsilon'_d/U \end{pmatrix}. \quad (4)$$

The prediction of Eqs. (3) and (4) is plotted in Fig. 3(a).  $(V_1^{(0)}, V_3^{(0)})$  describes the turning point of the position curve for the conductance peak in the gate voltage plane. It should be at the center of the type *c* line, which is constructed by extrapolating the positions of the (single-electron like) *a* and *b* lines into the regions of interaction. In Fig. 3(a) we see that the turning point  $(V_1^{(0)}, V_3^{(0)})$  is slightly offset by 0.13 mV in  $V_1$  (horizontally) and  $-0.05 \text{ mV}$  in  $V_3$  (vertically). This deviation indicates that the assumption of a Lorentzian spectral density for the strongly tunnel coupled dot simply being shifted by recharging the weakly coupled dot is not strictly fulfilled. Such an offset could be caused, for example, by an asymmetric spectral density and/or energy dependent tunnel barriers. However, apart from this small offset, the calculated curve reproduces the position shift of the conductance peak with good accuracy.

Predicting the value of the peak conductance is a much more difficult task. It varies along the position curve, reaching a minimum at the turning point. With increasing temperature, conductance decreases on all parts of the curve, notably at the turning point (Fig. 3(e)), so it is essential to calculate at finite temperature. To this end, we performed NRG calculations [14] for Hamiltonian (1) with experimentally predetermined parameters and taking into account a reduction of the tunnel couplings  $\Gamma_u, \Gamma_d$  by a factor of 2 because many-body effects

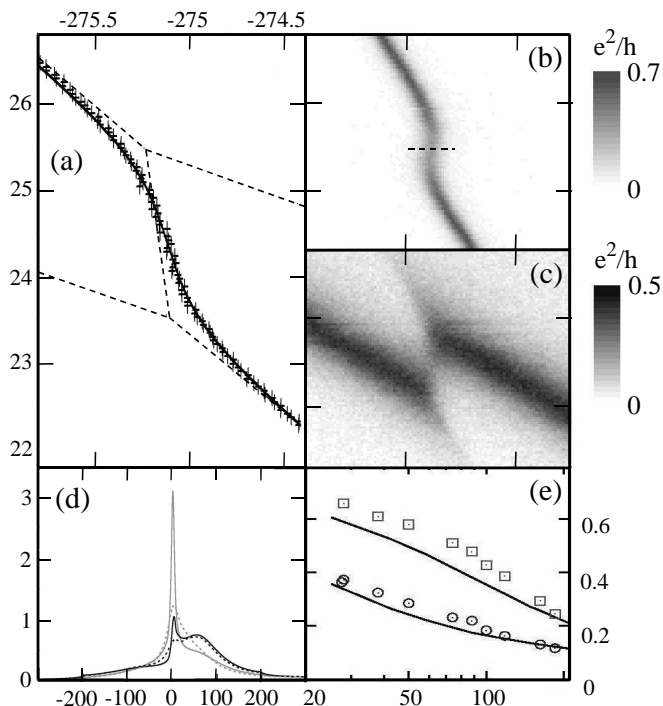


FIG. 3: (a) Crosses give the positions of conductance maxima in the upper dot, extracted from Fig. 2(b) (axes in mV). Solid line: prediction of Eq. (3), dashed line: honeycomb edges. (b),(c) Measured conductances of upper and lower dot around another type  $c$  line at 25 mK (axes like in Fig. 2). The measured parameters are  $\Gamma_u = 31 \mu\text{eV}$ ,  $\Gamma_d = 86 \mu\text{eV}$ ,  $U = 120 \mu\text{eV}$ . (d) NRG spectral densities  $A(\omega)$  at the middle of the dashed line in (b), showing the development of a Kondo resonance in both dots with decreasing temperature ( $A$  in  $\mu\text{eV}^{-1}$ ,  $\omega$  in  $\mu\text{eV}$ ). Grey: upper dot, black: lower dot. Solid:  $T = 25$  mK, dashed:  $T = 144$  mK. (e) Measured peak conductances (in  $e^2/h$ ) for two line cuts of (b) as a function of temperature (in mK). Boxes: Crossing the  $a$  line at fixed  $V_{1,2}$ , circles: crossing the  $c$  line at fixed  $V_{1,2}$  as shown in (b). The solid line give the respective NRG calculation results.

lead to an additional broadening of the side bands of the Anderson impurity model [15]. The NRG results for the region around the  $(N_u, N_d) = (0, 1)/(1, 0)$  boundary in Fig. 2 (c) and (e) agree well with experiment, including a reduced conductance around the turning points. Near the turning points of Fig. 2(e) and Fig. 3(b), an additional Kondo resonance develops at the Fermi level in the NRG spectra, see Fig. 3(d). Hence, for tunnel couplings  $\Gamma_u, \Gamma_d$  both tuned to intermediate values, we can trace back the conductance along the type  $c$  line to (orbital) Kondo tunnel processes still above the Kondo temperature. We also note two deviations if we restrain ourselves from adjusting the parameters: For the upper dot, the theoretical curve is somewhat smoother in the region of the type  $c$  line; for the lower dot the conductance peak height is lower since many-body effects lead to a transfer of spectral weight so that the behavior is more complicated than the simple shift of the Lorentzian-broadened

peak assumed when determining the tunnel rate. Both deviations could be reduced if the tunnel rate to the lower dot was reduced. Also effects beyond our calculation, in particular decoherence and the importance of more than one level in the lower dot, would lead to an adjustment in the same direction.

In conclusion, having full control over tunnel couplings and gate voltages of two laterally arranged quantum dots and measuring the conductance through the two dots separately, we were able to unambiguously identify regions of single-electron tunneling and correlated Kondo tunneling. Our experimental and theoretical analysis shows that the interdot Kondo effect leads to conductance through both dots in the region of the type  $c$  line if tunnel couplings are roughly symmetrical albeit the temperature is still slightly above the Kondo temperature.

We acknowledge helpful discussions with J. Bauer and Th. Pruschke, and thank Th. Pruschke for making available his NRG program. The project has been supported by the BMBF under grant 01BM455 and the DFG within the SFB/TRR21.

- 
- [1] C. Beenakker, Phys. Rev. B **44**, 1646 (1991).
  - [2] D. Goldhaber-Gordon *et al.*, Nature (London) **391**, 156 (1998); S. Cronenwett *et al.*, Science **281**, 540 (1998); J. Schmid *et al.*, Physica B (Amsterdam) 256-258, 182 (1998).
  - [3] L. I. Glazman and M. E. Raikh, JETP Lett. **47**, 452 (1988); T. K. Ng and P. A. Lee, Phys. Rev. Lett. **61**, 1768 (1988).
  - [4] U. Wilhelm *et al.*, Physica E (Amsterdam) **9**, 625 (2001).
  - [5] L. Borda *et al.*, Phys. Rev. Lett. **90**, 026602 (2003); T. Pohjola *et al.*, Europhys. Lett. **54**, 241 (2001).
  - [6] S. Sasaki *et al.*, Phys. Rev. Lett. **93**, 017205 (2004).
  - [7] P. Jarillo-Herrero *et al.*, Nature (London) **434**, 484 (2005).
  - [8] I. H. Chan *et al.*, Appl. Phys. Lett. **80**, 1818 (2002); D. T. McClure *et al.*, Phys. Rev. Lett. **98**, 056801 (2007).
  - [9] U. Wilhelm *et al.*, Physica E (Amsterdam) **14**, 385 (2002).
  - [10] A. Hübel *et al.*, Appl. Phys. Lett. **91**, 102101 (2007).
  - [11] W. G. van der Wiel *et al.*, Rev. Mod. Phys. **75**, 1 (2003).
  - [12] A. Hübel *et al.*, Physica E (Amsterdam) **40**, 1573 (2008).
  - [13] G. Mahan, Many-Particle Physics, 2nd ed., Plenum Press, New York (1990).
  - [14] K.G. Wilson, Rev. Mod. Phys. **47**, 773 (1975); H.R. Krishna-murthy, J.W. Wilkins, and K.G. Wilson, Phys. Rev. B **21**, 1003 (1980); *ibid.* **21**, 1044 (1980); Th. Pruschke and R. Bulla, Eur. Phys. J. B **44**, 217 (2005). The NRG discretization parameter chosen is  $\Lambda = 2.66$  ( $\Lambda < 2$ ) keeping 1100 (3600) states for Fig. 2 (Fig.3), conduction bandwidth is 400 eV; conductances are calculated via Y. Meir and N. S. Wingreen, Phys. Rev. Lett. **68**, 2512 (1992).
  - [15] The lifetime of a hole is enhanced by a factor 2 since there are two decay channels (spin up and down), see W. Brenig and K. Schönhammer, Z. Phys. **267**, 201-208

(1974).

[16] Here measured by lock-in technique with a modulation voltage of  $1 \mu\text{V}_{\text{pp}}$ .

[17] Please note, we define  $E_C = e^2/C_\Sigma$ , instead of  $E_C = e^2/2C_\Sigma$ .